Eur Radiol (2017) 27:4383–4393
DOI 10.1007/s00330-017-4782-3

HEPATOBILIARY-PANCREAS

The value of gadoxetic acid-enhanced MRI for differentiation between hepatic microabscesses and metastases in patients with periampullary cancer

Seo-Youn Choi[1] · Young Kon Kim[2] · Ji Hye Min[2,3] · Dong Ik Cha[2] · Woo Kyoung Jeong[2] · Won Jae Lee[2]

Received: 24 January 2017 / Revised: 14 February 2017 / Accepted: 16 February 2017 / Published online: 24 March 2017

Abstract

Objectives We aimed to identify features that differentiate hepatic microabscess from hepatic metastasis on gadoxetic acid-enhanced MRI in patients with periampullary cancer.

Methods We included 72 patients (31 patients with 83 hepatic microabscesses and 41 patients with 71 hepatic metastases) who had a history of periampullary cancer and underwent gadoxetic acid-enhanced MRI. Image analysis was performed for margin, signal intensity, rim enhancement, perilesional hyperaemia, pattern on DWI and dynamic phases, and size discrepancy between sequences by consensus of two observers.

Results Multivariate analysis revealed that the following significant parameters favour microabscess: a history of bile duct cancer, perilesional hyperaemia, persistent arterial rim enhancement through the transitional phase (TP), and size discrepancy between T1WI and T2WI and between T1WI and hepatobiliary phase image (HBPI). The diagnostic accuracy for microabscess was highest (90.9%) when showing a size discrepancy ≥30% between T1WI and HBPI or persistent arterial rim enhancement through the TP. When the lesion was positive for both these variables, specificity reached 100%.

Conclusion The combination of a size discrepancy between T1WI and HBPI and persistent arterial rim enhancement through the TP represents a reliable MRI feature for distinguishing between hepatic microabscess and metastasis in patients with periampullary cancer.

Key points

- *Gadoxetic acid-enhanced MRI is useful for distinguishing hepatic microabscess from metastasis.*
- *Hepatic microabscess showed significant size discrepancy ≥30% between T1WI and HBPI.*
- *Arterial rim enhancement persistent through the TP indicates hepatic microabscess.*

Keywords Liver · MRI · Abscess · Neoplasm metastasis · Contrast media · Hepatocyte-specific contrast

Abbreviations

DWI	Diffusion-weighted image
HBPI	Hepatobiliary phase image
MRI	Magnetic resonance imaging
PVP	Portal venous phase
SI	Signal intensity
T1WI	T1-weighted image
T2WI	T2-weighted image
TP	Transitional phase

Introduction

Hepatic abscess is a localized collection of necrotic inflammatory tissue in hepatic parenchyma caused by an infectious

Electronic supplementary material The online version of this article (doi:10.1007/s00330-017-4782-3) contains supplementary material, which is available to authorized users.

✉ Young Kon Kim
youngkon0707.kim@samsung.com

[1] Department of Radiology, Soonchunhyang University College of Medicine, Bucheon Hospital, Bucheon, Korea

[2] Department of Radiology and Center for Imaging Science, Samsung Medical Center, Sungkyunkwan University School of Medicine, 81 Ilwon-Ro, Gangnam-gu, Seoul 06351, Korea

[3] Department of Radiology, Chungnam National University Hospital, Chungnam National University College of Medicine, Daejeon, Korea

process. Distinctive imaging findings of hepatic abscess have been reported, including 'cluster sign' or 'double-target sign', on computed tomography (CT) and magnetic resonance imaging (MRI) [1–5]. The imaging features of hepatic metastasis have been well documented in extensive studies [6–9]. However, these two entities have several overlapping imaging features such as peripheral rim enhancement and diffusion restriction [3, 6, 10–12].

A study by Balci et al. [3] demonstrated arterial rim enhancement in hepatic abscesses that persisted into the delayed phase with negligible change in its degree and thickness on dynamic MRI with extracellular contrast media (ECCM). Choi et al. [10] reported that non-defect of arterial enhancing rim on a hepatobiliary phase image (HBPI) of gadoxetic acid (Primovist®, Bayer Healthcare, Berlin, Germany)-enhanced MRI suggested hepatic abscess rather than metastasis. Diffusion-weighted imaging (DWI) is also useful for the differential diagnosis of these two entities [6, 11]. Nevertheless, accurate differentiation of hepatic abscess from metastasis is still challenging, particularly when it is a small lesion in a patient with atypical clinical symptoms who has malignant biliary obstruction or underwent bile duct surgery, as both conditions are vulnerable to both microabscess and metastasis.

Gadoxetic acid, a liver-specific MR contrast agent, provides haemodynamic information during early dynamic phases similar to those of ECCM-MRI [13–17]. However, gadoxetic acid is taken into hepatocytes approximately 60–90 s after contrast injection, and thus the signal intensity (SI) on the portal venous phase (PVP) or transitional phase (TP; 3-min delay) is not exactly the same as that of ECCM-enhanced MRI [18, 19]. Given that SIs on the PVP or TP and HBPI of gadoxetic acid MRI comprise mixed extracellular existence and hepatocyte uptake, along with the peculiar characteristics of gadoxetic acid (i.e. usage of a lower dose and a shorter plasma half-life), we could surmise that imaging features of hepatic microabscess on early dynamic phases of gadoxetic acid MRI could be different from those on ECCM-MRI, which in turn would be helpful to distinguish microabscess from metastasis. In addition, several articles have reported that hepatic metastasis could show a target appearance on HBPI and/or DWI [6, 20].

In this context, we conducted this study to determine the imaging features that can be used to differentiate hepatic microabscess (2 cm or less in diameter) from metastasis on gadoxetic acid-enhanced MRI including DWI in patients with a history of underlying periampullary cancer.

Materials and methods

Patient population

The institutional review board approved the study and waived the requirement for informed consent because of the retrospective design of this study. We retrospectively queried the radiological data for patients who had been diagnosed with periampullary cancer and undergone liver MRI having the terms 'abscess' or 'metastasis' on radiological MR reports between January 2010 and September 2015. As a result, we found a total of 502 patients with periampullary cancers suspected of having abscess or metastasis in the liver. Of these 502 patients, 223 patients had no focal hepatic lesion and an additional 207 patients were excluded for the following reasons: MRI findings typical of a cystic lesion ($n = 179$), large abscess or metastasis (>2 cm in diameter) ($n = 19$), lost to follow-up in cases without a confirmed abscess or metastasis ($n = 6$) and poor image quality ($n = 3$). Finally, 31 patients with hepatic abscesses 2 cm or smaller in size (21 males and 10 females, mean age 66.71 years; age range, 48–85 years) and 41 patients with hepatic metastases 2 cm or smaller (26 males and 15 females, mean age 61.85 years; age range, 44–85 years) were enrolled in this study. Among the enrolled total 72 patients, 20 patients had no history of previous operation for periampullary malignancy at the time of MR examination and the remaining 52 patients was in a postoperative period. Among the 20 patients without history of previous operation, eight patients received surgical resection after MR examination and the remaining 12 patients had not received surgery at all.

All periampullary cancers were pathologically proven by surgery ($n = 60$) or biopsy ($n = 12$). The types of surgery were as follows: pylorus-preserving pancreaticoduodenectomy ($n = 424$), Whipple's operation ($n = 17$) and total pancreatectomy ($n = 1$). A total of 83 microabscesses (mean size, 0.8 cm; standard deviation, 0.6 cm) were identified in the 31 patients, as follows: 18 patients had one or two lesions, five patients had three lesions, two patients had four lesions, and the remaining six patients had five or more lesions (five to eight). Among the 31 patients in the microabscess group, ten patients had pathologically proven microabscesses by biopsy and the remaining 21 patients were clinically diagnosed as the lesions disappeared or decreased in size with antibiotic treatment during follow-up. Forty-one patients had 71 hepatic metastases (mean size, 1.2 cm; standard deviation, 0.8 cm) as follows: 23 patients had one solitary lesion, ten patients had two lesions, six patients had three lesions and the remaining two patients had five lesions. Among 41 patients in the metastasis group, 21 patients with were pathologically diagnosed by surgery in five patients who had single metastasis detected on follow-up imaging or biopsy in 16 patients and the remaining 20 patients were clinically diagnosed based on increase or decrease in size on follow-up CT or MRI after chemotherapy. For patients with multiple lesions, sonography-guided biopsy was performed for only one or two liver lesions because the imaging features of multiple liver lesions were identical in each patient. The case accrual process is summarised in Fig. 1.

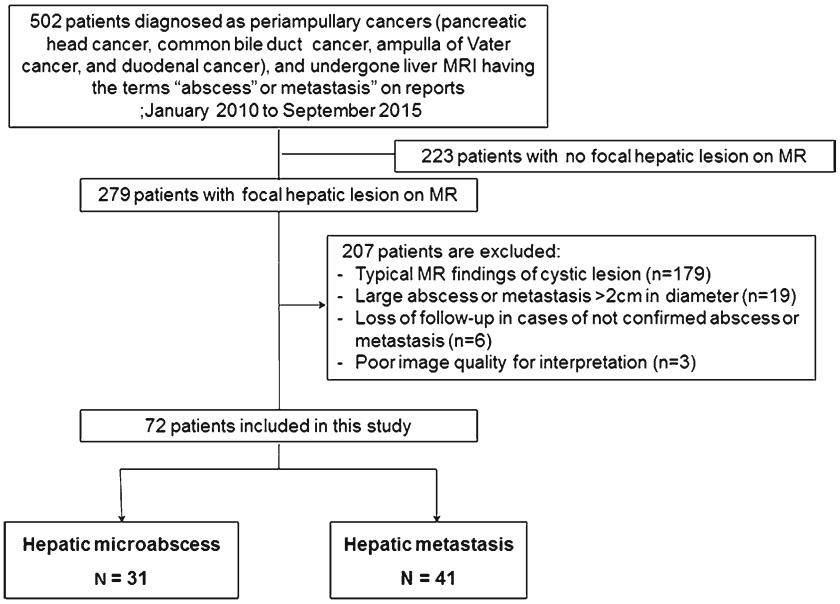

Fig. 1 Flow chart of the study population

Twelve patients in the metastasis group and seven patients in the microabscess group showed elevation of total or direct bilirubin (normal range: <1.2 mg/dl and <0.4 mg/dl, respectively). Laboratory findings at the time of MR examinations are shown in Supplementary Table 1.

MRI examination

MRI was performed using a 3.0-T whole-body MRI system (InteraAchieva 3.0 T; Philips Healthcare, Best, The Netherlands) with a 16-channel phased-array coil as the receiver coil. Baseline MRI included a T1-weighted turbo field-echo in-phase and opposed-phase sequence, and a respiratory-triggered single-shot T2-weighted image (T2WI) and heavy T2WI (Table 1). Unenhanced and gadoxetic acid-enhanced arterial phase (AP, 20–35 s), PVP (60 s), TP (3 min) and HBPI (20 min) were acquired using a T1-weighted 3D turbo-field-echo sequence (enhanced T1 high-resolution isotropic volume examination; eTHRIVE, Philips Healthcare). The contrast agent was administered intravenously at a dose of 0.025 mmol/kg (0.1 ml/kg body weight) at a rate of 2 ml/s using a power injector (Mark V; Medrad, Indianola, PA, USA) and was immediately followed by 20-ml saline flush. DWI was obtained using single-shot echo-planar imaging with respiratory triggering. *B*-values of 0, 100 and 800 s/mm^2 were used. The apparent diffusion coefficient (ADC) was calculated using a monoexponential function with *b*-values of 100 and 800 s/m^2.

Qualitative and quantitative analysis

All MRIs were reviewed by two abdominal radiologists (with 8 and 15 years of experience, respectively, in abdominal MRI interpretation) in consensus on a picture archiving and communication system (PACS; Centricity Radiology RA 1000; GE Healthcare, Chicago, IL, USA). Both observers were blinded to the clinical or histopathological results of each case. MRIs of both groups were presented randomly in a blinded

Table 1 MRI sequences and parameters

Sequence	TR/TE (m/sec)	Flip angle (degrees)	Section thickness	Matrix size	Bandwidth (Hz/pixel)	Field of view (cm)	Acquisition time (s)	No. of excitations
T1W- 2D dual GRE	3.5/1.15–2.3	10	6	256 × 194	434.4	32–38	14	1
RT-SS-T2WI	1342/80	90	5-7	320 × 256	506.4	32–38	-	2
RT-SS-HT2WI	1156/160	90	5-7	320 × 256	317.9	32–38	-	2
T1W-3D GRE	3.1/1.5	10	2	256 × 256	995.7	32–38	16.6	1
DWI	1600/70	90	5	112 × 112	79.5	30–38	-	2

TR repetition time, *TE* echo time, *T1W* T1-weighted, *GRE* gradient echo, *RT-SS-T2WI* respiration-triggered single-shot T2-weighted image, *RT-SS-HT2WI* respiration-triggered single-shot heavily T2-weighted image, *DWI* diffusion-weighted imaging

manner to avoid bias. After the first independent image analysis, interobserver agreement was assessed for MRI features. Thereafter, the two reviewers met to make final decisions by consensus for discordant cases.

For qualitative analysis, the following imaging parameters were evaluated: (a) margin (well-defined or fuzzy-margined), (b) multiplicity (single or multiple; two or more lesions), (c) rim enhancement on each phase of dynamic contrast-enhanced imaging (AP, PVP and TP), (d) perilesional hyperaemia on AP imaging, and (d) low SI rim on HBPI. The SI of the lesion on unenhanced, contrast-enhanced MRI and DWI (*b*-value of 800 s/mm^2) with ADC map was also recorded with categorization into three groups of hypo-, iso- or hyper-SI compared with unaffected liver parenchyma. The enhancement pattern was subcategorized into three groups: (a) arterial rim enhancement persistent through the TP, (b) arterial rim enhancement that disappeared at the TP, and (c) absence of rim enhancement on all phases of dynamic image. DWI pattern was subdivided into two groups: (a) homogeneously high SI relative to liver parenchyma through the whole area of the focal hepatic lesion, and (b) high SI rim confined to the periphery of focal hepatic lesion, with relatively lower SI in the centre.

Lesion size measurement was done by an abdominal radiologist who did not participate in the qualitative image analysis. We chose T1-weighted image (T1W1), T2WI and HBPI in consideration of the fact that inflammatory lesions tend to look smaller on T1WI and larger on T2WI or HBPI with the naked eye [6, 20]. The presence of a significant size discrepancy was defined when the longest diameter of the lesion on unenhanced T1WI was ≥30% smaller than that on T2WI or HBPI with consideration for intra-individual and interindividual variability in measuring the size of small hepatic lesions. When the lesions were invisible on unenhanced T1WI, they were categorised as having a size discrepancy.

Statistical analysis

The chi-square test or Fisher's exact test was used to compare the frequency of categorical variables for differentiation of hepatic microabscess and metastasis. Student's *t*-test or the Wilcoxon rank sum test was performed for continuous variables. To determine the predictors of hepatic microabscess, multivariable logistic regression analyses were conducted with backward selection using significant variables on univariate analysis. Then, from variables that were significant on multivariable analysis, we chose two categories showing the highest diagnostic accuracy compared to the remaining variables. The sensitivity, specificity and accuracy of each imaging finding and combinations of findings were also calculated. Interobserver agreement was analysed for each variable using k statistics and interpreted as: poor, <0.20; fair, 0.20–0.39; moderate, 0.40–0.59; substantial, 0.60–0.79; and almost perfect, 0.80. All statistical analyses were performed using SPSS version 20.0 (SPSS Inc., Chicago, IL, USA) and MedCalc version 16.4.3. (MedCalc Software, Mariakerke, Belgium).The significance level was set to $P < 0.05$ (two-tailed).

Results

Twenty-four microabscess and ten metastasis were identified in 13 (41.9%) and seven patients (17.1%) with no history of previous surgery for periampullary malignancy, respectively. In the remaining 52 patients, a microabscess ($n = 18$, 58.1%) or metastasis ($n = 34$, 82.9%) was found on follow-up MRI after surgery for periampullary cancer. Among the 20 patients without a history of previous surgery, upstream biliary dilatation due to periampullary cancer was found in nine patients with microabscess and six patients with metastasis.

Table 2 summarizes all of the evaluated parameters for distinguishing hepatic microabscess and metastasis and representative images are shown in Figs. 2, 3 and 4. Hepatic microabscess was more frequently observed than hepatic metastasis, when the primary malignancy was common bile duct cancer rather than ampulla of Vater cancer or pancreatic head cancer ($P = 0.001$), and when the patient had a history of previous surgery for periampullary malignancy ($P = 0.039$). The margin of the lesion was significantly different between the two groups in all MRI sequences ($P < 0.001$). Perilesional hyperaemia on AP image was more frequently seen on hepatic microabscess than on metastasis ($P < 0.001$). Rim enhancements on AP, PVP and TP imaging were more frequently seen in hepatic microabscess than in metastasis ($P = 0.002$, $P < 0.001$ and $P < 0.001$, respectively). Only four of 41 hepatic metastases showed rim enhancement on TP imaging. Among 80 hepatic microabscesses and 56 hepatic metastases with arterial rim enhancement, the rim enhancement disappeared on TP imaging in 29 hepatic microabscesses and 51 hepatic metastases. Furthermore, three of 83 hepatic microabscesses (3.6%) and 15 of 71 hepatic metastases (21.1%) showed no rim enhancement on any phases of the dynamic scan. Although the SI on DWI was not significantly different between the two groups, the low SI on the ADC map was more frequently observed in metastasis than in microabscess (83.1% vs. 26.5%, $P < 0.001$). With regard to the SI pattern on DWI, no hepatic microabscess showed a high SI rim on peripheral portion, while 39 hepatic metastases (54.9%) presented with a high SI rim mimicking target appearance ($P < 0.001$). Similarly, no hepatic microabscesses showed a low SI rim on HBPI and 17 metastases (41.5%) showed such a finding ($P < 0.001$).

The mean size of the microabscesses was largest on HBPI (1.48 ± 0.64 cm), followed by T2WI (1.46 ± 1.42 cm), AP (1.42 ± 1.33 cm), PVP (1.10 ± 1.08 cm), TP (0.96 ± 1.21 cm) and T1WI (0.88 ± 1.10 cm). The mean size of metastasis was

Table 2 Characteristics and univariable analysis of hepatic microabscess and metastasis with gadoxetic acid-enhanced MRI with DWI

Variable		Abscess	Metastasis	Total	*K* value	*P* value[a]
By patient		N = 31	N = 41	N = 72		
Demographic factors	Sex					0.895
	Male	21 (67.7%)	26 (63.4%)	47 (65.3%)		
	Female	10 (32.3%)	15 (36.6%)	25 (34.7%)		
	Primary cancer					0.001
	PHAC	12 (38.7%)	21 (51.2%)	33 (45.8%)		
	CBD cancer	16 (51.6%)	5 (12.2%)	21 (29.2%)		
	AoV cancer	3 (9.7%)	15 (36.6%)	18 (25.0%)		
	History of operation					0.039
	Absence	13 (41.9%)	7 (17.1%)	20 (27.8%)		
	Presence	18 (58.1%)	34 (82.9%)	52 (72.2%)		
	Multiplicity					0.681
	Single	15 (48.4%)	23 (56.1%)	38 (52.8%)		
	Multiple	16 (51.6%)	18 (43.9%)	34 (47.2%)		
By lesion		N = 83	N = 71	N = 154		
Baseline factors	Margin				0.68	<0.001
	Well-defined	0 (0.0%)	61 (85.9%)	61 (39.6%)		
	Fuzzy	83 (100.0%)	10 (14.1%)	93 (60.4%)		
Signal intensity (SI)	T1WI				0.96	0.007
	Hypo	73 (88.0%)	71 (100.0%)	144 (93.5%)		
	Iso	10 (12.0%)	0 (0.0%)	10 (6.5%)		
	T2WI				0.93	0.547
	Iso	2 (2.4%)	0 (0.0%)	2 (1.3%)		
	Hyper	81 (97.6%)	71 (100.0%)	152 (98.7%)		
	Arterial phase				0.82	<0.001
	Hypo	25 (30.1%)	58 (81.7%)	83 (53.9%)		
	Iso	1 (1.2%)	2 (2.8%)	3 (1.9%)		
	Hyper	57 (68.7%)	11 (15.5%)	68 (44.2%)		
	Portal phase				0.75	<0.001
	Hypo	59 (71.1%)	71 (100.0%)	130 (84.4%)		
	Iso	7 (8.4%)	0 (0.0%)	7 (4.5%)		
	Hyper	17 (20.5%)	0 (0.0%)	17 (11.0%)		
	Transitional phase				0.85	0.01
	Hypo	73 (88.0%)	71 (100.0%)	144 (93.5%)		
	Iso	7 (8.4%)	0 (0.0%)	7 (4.5%)		
	Hyper	3 (3.6%)	0 (0.0%)	3 (1.9%)		
	Hepatobiliary phase				0.90	0.302
	Hypo	80 (96.4%)	71 (100.0%)	151 (98.1%)		
	Iso	3 (3.6%)	0 (0.0%)	3 (1.9%)		
	DWI				0.95	0.27
	Hypo	1 (1.2%)	0 (0.0%)	1 (0.6%)		
	Iso	2 (2.4%)	0 (0.0%)	2 (1.3%)		
	Hyper	80 (96.4%)	71 (100.0%)	151 (98.1%)		
	ADC map				0.88	<0.001
	Hypo	22 (26.5%)	59 (83.1%)	81 (52.6%)		
	Iso	52 (62.7%)	12 (16.9%)	64 (41.6%)		
	Hyper	9 (10.8%)	0 (0.0%)	9 (5.8%)		
Perilesional hyperaemia (AP)	Absence	22 (26.5%)	55 (77.5%)	77 (50.0%)	0.74	<0.001
	Presence	61 (73.5%)	16 (22.5%)	77 (50.0%)		

Table 2 (continued)

Variable		Abscess	Metastasis	Total	*K* value	*P* value[a]
Rim enhancement	Arterial phase				0.86	0.002
	Absence	3 (3.6%)	15 (21.1%)	18 (11.7%)		
	Presence	80 (96.4%)	56 (78.9%)	136 (88.3%)		
	Portal phase				0.78	<0.001
	Absence	25 (30.1%)	51 (71.8%)	76 (49.4%)		
	Presence	58 (69.9%)	20 (28.2%)	78 (50.6%)		
	Transitional phase				0.82	<0.001
	Absence	28 (33.7%)	66 (93.0%)	94 (61.0%)		
	Presence	55 (66.3%)	5 (7.0%)	60 (39.0%)		
Rim enhancement pattern	Arterial rim persistent through the TP	51 (61.4%)	5 (7.0%)	56 (36.4%)	0.83	<0.001
	Arterial rim disappearance on TP	29 (34.9%)	51 (71.8%)	80 (51.9%)		
	No rim on any phase	3 (3.6%)	15 (21.1%)	18 (11.7%)		
DWI pattern	Homogeneous SI	31 (37.3%)	30 (42.3%)	61 (39.6%)	0.78	<0.001
	Peripheral high SI rim	0 (0.0%)	39 (54.9%)	39 (25.3%)		
	Centre high	52 (62.7%)	2 (2.8%)	54 (35.1%)		
Low SI rim on HBPI	Absence	83 (100.0%)	27 (38.0%)	110 (71.4%)	0.85	<0.001
	Presence	0 (0.0%)	44 (62.0%)	44 (28.6%)		
Size discrepancy[b]	Percentage change in size from T1 to T2				0.62	<0.001
	< 30%	53 (63.9%)	68 (95.8%)	121 (78.6%)		
	≥ 30%	30 (36.1%)	3 (4.2%)	33 (21.4%)		
	Percentage change in size from T1 to HBP				0.70	<0.001
	< 30%	35 (42.2%)	69 (97.2%)	104 (67.5%)		
	≥ 30%	48 (57.8%)	2 (2.8%)	50 (32.5%)		

Data are no. (%)

PHAC pancreatic head adenocarcinoma, *CBD* common bile duct, *AoV* ampulla of Vater, *T1WI* T1-weighted image, *T2WI* T2-weighted image, *DWI* diffusion weighted image, *ADC* apparent diffusion coefficient, *AP* arterial phase, *TP* transitional phase, *SI* signal intensity, *HBPI* hepatobiliary phase image

[a] *P*-values were derived from the chi-square test or Fisher's exact test as appropriate

[b] Percent change in size from A to B was defined as follows: (Size at B − Size at A)/Size at A × 100 if Size at A ≠ 0 and over 30% if Size at A = 0

largest on HBPI (1.35 ± 0.48 cm), followed by T2WI (1.32 ± 0.52 cm), AP (1.31 ± 0.52 cm), PVP (1.29 ± 0.57 cm), TP (1.25 ± 0.48 cm) and T1WI (1.08 ± 0.50 cm). Several microabscesses showed a size discrepancy of ≥ 30% between T1WI and T2WI (30/83; 36.1%), and between T1WI and HBPI (48/83; 57.8%). Most cases of hepatic metastasis showed a size discrepancy <30% between T1WI and T2WI, and between T1WI and HBPI (95.8% and 97.2%, respectively; $P < 0.001$). Interobserver agreement for all imaging findings was substantial to perfect ($k = 0.68$–0.96).

Table 3 shows the odds ratio (OR), sensitivity, specificity and accuracy of each significant MRI category for diagnosing hepatic microabscess by differentiating it from hepatic metastasis. Of the MRI categories that were significant on multivariable analysis, a size discrepancy ≥30% between T1WI and HBPI, and arterial rim enhancement persistent through the TP were the two categories that showed superior diagnostic accuracy (76.0% and 76.0%, respectively) compared to the remaining categories (range, 35.1–75.3%).

Table 4 shows the sensitivity, specificity, and accuracy of variable combinations of two significant MRI categories for diagnosing hepatic microabscess by differentiating it from hepatic metastasis. When the lesion was positive for a size discrepancy ≥30% between T1WI and HBPI or arterial rim enhancement persistent through the TP, there was 91.6% sensitivity, 90.1% specificity and 90.9% accuracy for a diagnosis of hepatic microabscess. When the lesion was positive for both categories, the specificity was 100%.

Discussion

This study showed that, among the significant MRI categories, a size discrepancy ≥30% between T1WI and HBPI and arterial rim enhancement persistent through the TP were found to show a higher diagnostic accuracy (76.0% and 76.0%, respectively) compared to the remaining categories (range, 35.1–75.3%) for diagnosing hepatic microabscess over

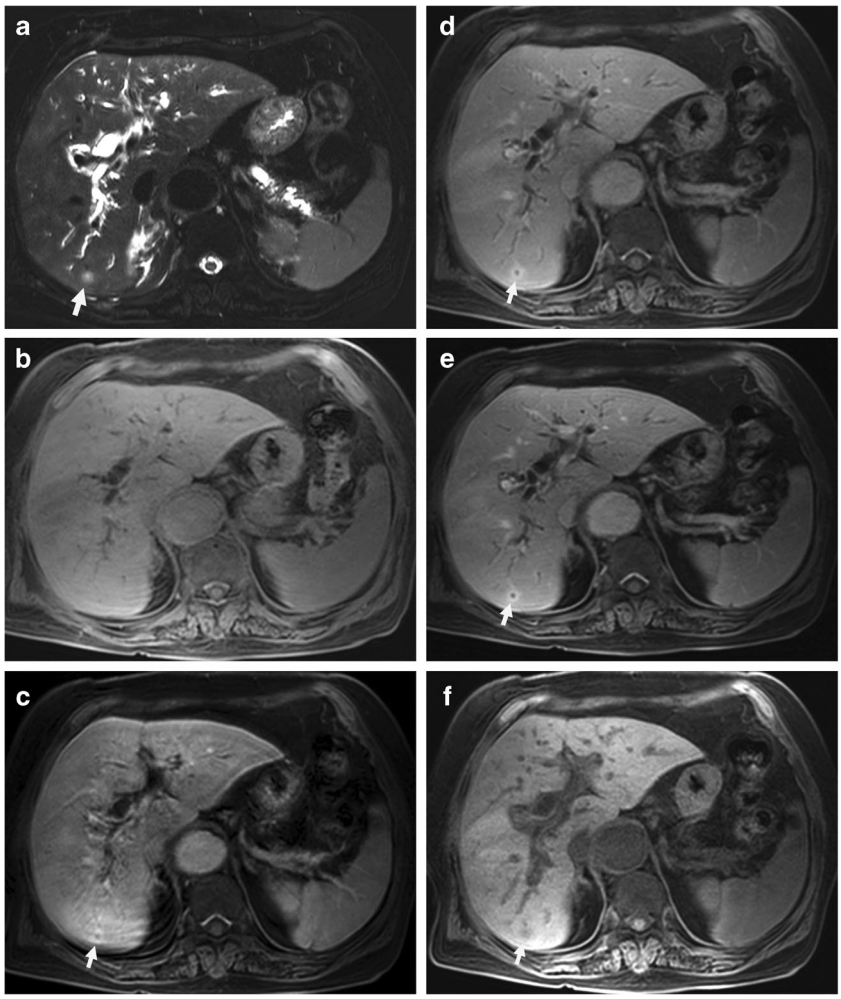

Fig. 2 A 59-year-old woman with pancreatic head cancer and hepatic microabscess. T2-weighted imaging (**a**) shows a well-defined hyperintense lesion (arrow) in segment VI. Intrahepatic biliary dilatation is noted due to underlying pancreatic head cancer. In the unenhanced T1-weighted imaging (**b**), the lesion is not clearly depicted. Gadoxetic acid-enhanced dynamic images (**c**–**e**) show persistent rim enhancement from the arterial phase (**c**) through the portal (**d**) and transitional phases (**e**). Hepatobiliary phase imaging obtained 20 min after injection of contrast agent (**f**) shows an ill-defined faint hypointense lesion (arrow). As the lesion is invisible on T1-weighted imaging (**b**), it was regarded as having a size discrepancy between T1-weighted imaging and hepatobiliary phase imaging

metastasis. When the lesion was positive for any one of these two categories, the sensitivity reached 91.6%. Furthermore, when the lesion was positive for both categories, the specificity reached 100%, which has important clinical implications because accurate characterization of hepatic metastasis is relevant to patient outcome.

Our results revealed that the presence of a size discrepancy ≥30% between T1WI and HBPI was a significant indicator of hepatic microabscess rather than hepatic metastases. This is in line with several previous reports regarding the differentiation between eosinophilic abscess and hepatic metastasis [21, 22]. Theoretically, perfusion abnormalities and inflammatory changes around the focal inflammatory hepatic lesion could lead to functional ischaemia due to decreased portal perfusion, and in turn decreased hepatocyte function of variable degrees [22]. This phenomenon could explain why the mean size of microabscess and metastasis was largest on HBPI among variable MRI sequences in our study. Meanwhile, precontrast T1WI seems to be the least sensitive at delineating hepatic inflammatory process [21], and microabscess is likewise poorly perceptible on T1WI.

The presence of rim enhancement on TP imaging was an independently significant variable for predicting hepatic microabscess versus metastasis ($P < 0.001$). Weighting on the dynamic pattern of arterial rim enhancement, persistent rim enhancement through the TP suggested hepatic microabscess, whereas no rim enhancement on TP imaging or disappearance of arterial rim enhancement on TP imaging suggested hepatic metastasis. The mechanism of this phenomenon is difficult to elucidate due to complex mechanisms of mixed extracellular existence and hepatocyte uptake of gadoxetic acid. We surmised that the fibro-inflammatory process accompanying vascular-rich granulation tissue in the periphery of the abscess, in which hepatocyte function begins to recover, is responsible for persistent rim enhancement. Meanwhile, the weaker dynamic phases of gadoxetic acid (i.e. nearly a quarter dose of gadolinium in gadoxetic acid with a short plasma half-life compared to the conventional ECCM gadolinium agent) taken together with early hepatocyte contrast uptake, and underlying malignant biliary obstruction, might pervert the classic enhancement feature of metastasis seen on ECCM-MRI as haemangioma frequently appears as

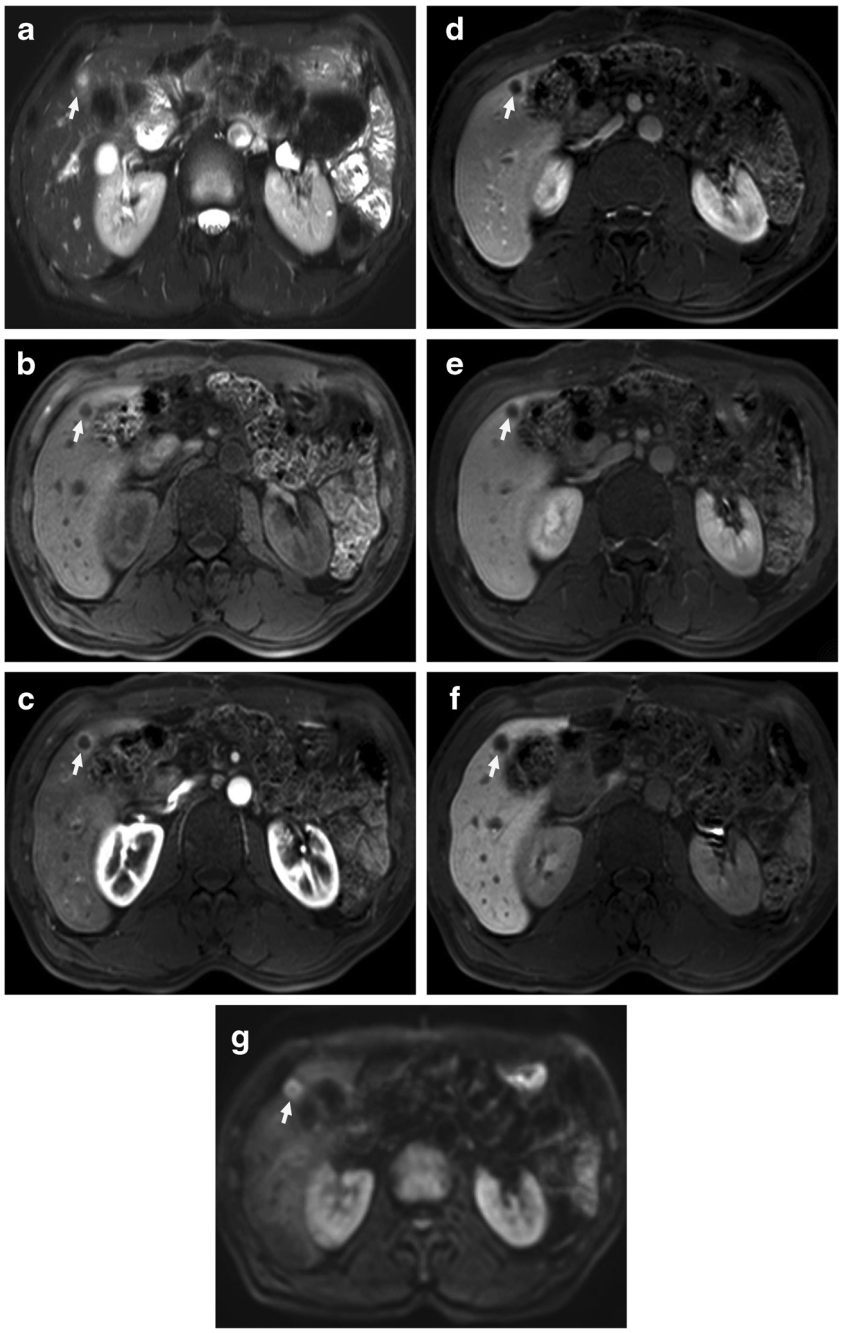

Fig. 3 A 53-year-old man with common bile duct cancer and hepatic metastasis. T2-weighted imaging (**a**) shows fuzzy hyperintense lesion (arrow) in segment V. Unenhanced T1-weighted imaging (**b**) shows a well-defined hypointense lesion (arrow). In gadoxetic acid-enhanced dynamic imaging (**c**–**e**), rim enhancement is seen on arterial phase image (**c**) and disappears through the portal (**d**) and transitional phases (**e**). Hepatobiliary phase imaging obtained 20 min after injection of contrast agent (**f**) shows a well-defined hypointense lesion (arrow). Diffusion-weighted imaging (**g**) shows a peripheral high-signal intensity rim with central darker area. The size difference between T1-weighted imaging (10.1 mm) and hepatobiliary phase imaging (11.2 mm) was not remarkable (1.1 mm)

hypointensity on 3-min TP imaging, mimicking the washout sign of hypervascular hepatocellular carcinoma [18, 19].

Interestingly, 29 microabscesses with disappearance of arterial rim enhancement on TP imaging were seen as a nodular area of dark SI, which was smaller than on the AP, PVP and HBPI, due to transition of an early rim-like enhanced area into isointensity on the TP (Fig. 4). This explains the smaller measured lesion size on TP imaging after T1WI compared to other images. This is in partial agreement with the previous study [10], which has demonstrated that arterial rim enhancement in most abscesses (85.7%) remained enhanced on HBPI, which was referred to as 'non-defect' of arterial enhancing rim on HBPI. We could not apply this feature in the statistical analysis because it was confined to lesions showing arterial rim enhancement. Since no metastases in our case series showed such a feature, we expect that applying isointensity of arterial rim enhancement on TP imaging could lead to a better diagnostic accuracy for characterizing microabscess than the current value.

When examining the pattern on DWI, a peripheral high SI rim was observed only in hepatic metastasis ($n = 39$, 54.9%),

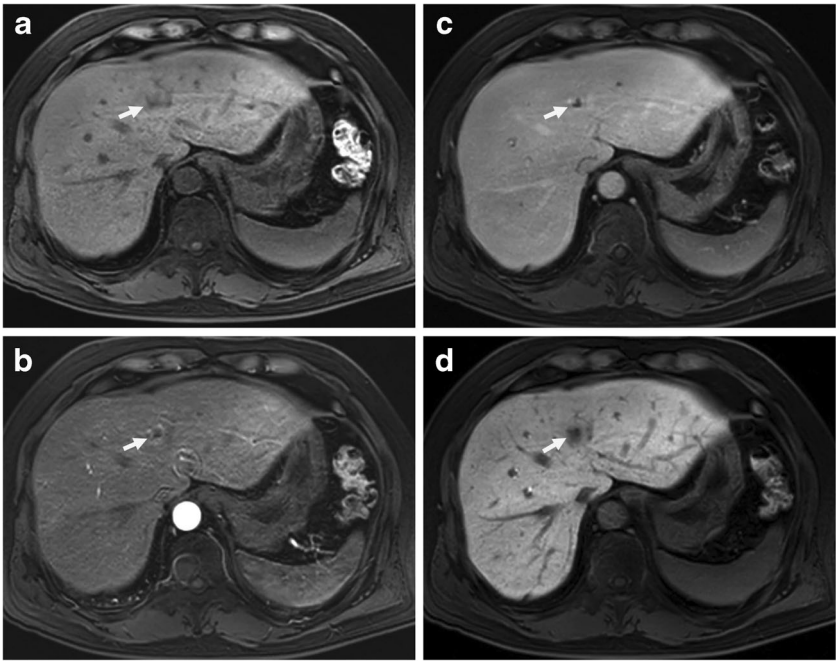

Fig. 4 A 57-year-old man with ampulla of Vater cancer and hepatic microabscess. Unenhanced T1-weighted imaging (**a**) shows an ill-defined subtle hypointensity in segment IV (arrow). In gadoxetic acid-enhanced dynamic imaging (**b, c**), rim enhancement (arrow) is seen on the arterial phase image (**b**) and disappears (arrow) in the transitional phase (**c**) due to the isointensity surrounding the liver parenchyma. Hepatobiliary phase imaging obtained 20 min after injection of gadoxetic acid (**d**) clearly shows a hypointense lesion that is larger than seen on the unenhanced T1-weighted imaging (**a**)

and not in microabscess. Similarly, a peripheral low SI rim on HBP was also observed only in metastasis ($n = 44$, 62.0%), consistent with previous reports [18, 19, 23] that demonstrated the target sign of liver metastasis from breast cancer or colorectal cancer. Thus, our study reaffirmed the utility of the target sign on HBPI or DWI for characterizing hepatic metastasis,

Table 3 Diagnostic performance of each variable for differentiating hepatic microabscess from metastasis

Variable	Abscess (n =83)	Metastasis (n =71)	Univariable logistic regression		Multivariable logistic regression		Sensitivity (%) (95% CI)	Specificity (%) (95% CI)	Accuracy (%) (95% CI)
			OR (95% CI)	*P* value	OR (95% CI)	*P* value			
Primary cancer							49.4 (38.2–60.6)	18.3 (10.1–29.3)	35.1 (27.6–43.2)
PHAC	42	13	1 (Ref.)		1 (Ref.)				
CBD cancer	5	20	0.08 (0.02–0.25)	<0.001	0.18 (0.02–1.52)	0.117			
AoV cancer	36	38	0.29 (0.14–0.63)	0.002	0.1 (0.02–0.46)	0.003			
Perilesional hyperaemia on AP							73.5 (62.7–82.6)	77.5 (66–86.5)	75.3 (67.7–81.9)
Absence	22	55	1 (Ref.)		1 (Ref.)				
Presence	61	16	9.53 (4.55–19.98)	<0.001	5.74 (1.42–23.26)	0.014			
Persistent rim through the TP							61.4 (50.1–71.9)	93.0 (84.3–97.7)	76.0 (68.4–82.5)
Absence	32	66	1 (Ref.)		1 (Ref.)				
Presence	51	5	21.04 (7.66–57.8)	<0.001	53.45(10.24–278.9)	<0.001			
Size discrepancy between T1WI and T2WI							36.1 (25.9–47.4)	95.8 (88.1–99.1)	63.6 (55.5–71.2)
< 30%	53	68	1 (Ref.)		1 (Ref.)				
≥ 30%	30	3	12.83(3.71–44.32)	<0.001	0.08 (0–4.22)	0.211			
Size discrepancy between T1WI and HBPI							57.8 (46.5–68.6)	97.2 (90.2–99.7)	76.0 (68.4–82.5)
< 30%	35	69	1 (Ref.)		1 (Ref.)				
≥ 30%	48	2	47.31(10.86–206.08)	<0.001	1102.33 (12.96–93791.47)	0.002			

PHAC pancreatic head adenocarcinoma, *CBD* common bile duct, *AoV* ampulla of Vater, *AP* arterial phase, *TP* transitionalphase, *T1WI* T1-weighted image, *T2WI* T2-weighted image, *HBPI* hepatobiliary phase image, *OR* odds ratio, *CI* confidence interval

Table 4 Diagnostic performance of MRI features for identifying hepatic microabscess

Combination	Per lesion analysis			Per patient analysis		
	Sensitivity (%) (95% CI)	Specificity (%) (95% CI)	Accuracy (%) (95% CI)	Sensitivity (%) (95% CI)	Specificity (%) (95% CI)	Accuracy (%) (95% CI)
Category 1[a]	57.8 (46.5–68.6)	97.2 (90.2–99.7)	76.0 (68.4–82.5)	67.7 (51.6–83.9)	97.6 (92.7–100)	84.7 (76.4–91.7)
Category 2[b]	61.4 (50.1–71.9)	93.0 (84.3–97.7)	76.0 (68.4–82.5)	58.1 (38.7–74.2)	90.2 (80.5–97.6)	76.4 (66.7–84.7)
Category 1 or 2	91.6 (83.4–96.5)	90.1 (80.7–95.9)	90.9 (85.2–94.9)	90.3 (74.2–98)	87.8 (73.8–95.9)	88.9 (79.3–95.1)
Category 1 plus 2	27.7 (18.4–38.6)	100 (94.9–100)	61 (52.9–68.8)	35.5 (19.2–54.6)	100 (91.4–100)	72.2 (60.4–82.1)

CI confidence interval

[a] Category 1: Size discrepancy between T1-weighted image and hepatobiliary phase image

[b] Category 2: Arterial rim enhancement persistent through the transitional phase

although those features were not included in our multivariate analysis. Given intrahepatic cholangiocarcinoma and metastasis might have central fibrous stroma and necrosis, the central enhancing area on HBP and a central area of darker SI on DWI could be explained by increased diffusivity of the contrast medium within the area of central necrosis and/or persistent contrast uptake in fibrotic stroma with abundant interstitial space.

Our study had some limitations. First, as this study was a retrospective review of select patients groups, there was an inevitable selection bias. Since only patients who had an underlying history of periampullary cancer were included, our results might not be applicable to other underlying diseases. Second, not all lesions were confirmed histologically. However, for the lesions not pathologically confirmed, we tried to include only strongly suspected abscesses and metastases based on the aforementioned criteria to minimize false-negative or false-positive cases. Third, we did not assess the diagnostic performance of suggested criteria for diagnosing hepatic microabscess over small metastasis.

In conclusion, in gadoxetic acid-enhanced MRI, the combination of a size discrepancy between T1WI and HBPI and arterial rim enhancement persistent through the TP could be reliable MRI criteria for characterizing hepatic microabscess from metastasis in patients with a history of periampullary cancer. The combination of these two categories led to 100% specificity for differentiating hepatic microabscess from metastasis.

Acknowledgements The scientific guarantor of this publication is Won Jae Lee, the head of the Radiology Department of Samsung Medical Center. The authors of this manuscript declare no relationships with any companies whose products or services may be related to the subject matter of the article. This research did not receive any specific grant from funding agencies in the public, commercial or not-for-profit sectors. This work was supported by the Soonchunhyang University Research Fund. Bo ra Lee kindly provided statistical advice for this study. Institutional Review Board approval was obtained. Written informed consent was waived by the Institutional Review Board because of the retrospective nature of the study. No study subjects or cohorts have been previously reported. Methodology: retrospective, observational, performed at one institution.

References

1. Jeffrey RB Jr, Tolentino CS, Chang FC, Federle MP (1988) CT of small pyogenic hepatic abscesses: The cluster sign. AJR Am J Roentgenol 151:487–489
2. Mathieu D, Vasile N, Fagniez PL, Segui S, Grably D, Larde D (1985) Dynamic CT features of hepatic abscesses. Radiology 154: 749–752
3. Balci NC, Semelka RC, Noone TC et al (1999) Pyogenic hepatic abscesses: MRI findings on T1- and T2-weighted and serial gadolinium-enhanced gradient-echo images. J Magn Reson Imaging 9:285–290
4. Garcia-Eulate R, Hussain N, Heller T et al (2006) CT and MRI of hepatic abscess in patients with chronic granulomatous disease. AJR Am J Roentgenol 187:482–490
5. Vilgrain V, Esvan M, Ronot M, Caumont-Prim A, Aube C, Chatellier G (2016) A meta-analysis of diffusion-weighted and gadoxetic acid-enhanced MR imaging for the detection of liver metastases. Eur Radiol 26:4595–4615
6. Park HJ, Kim SH, Jang KM, Lee SJ, Park MJ, Choi D (2013) Differentiating hepatic abscess from malignant mimickers: Value of diffusion-weighted imaging with an emphasis on the periphery of the lesion. J Magn Reson Imaging 38:1333–1341
7. Zech CJ, Herrmann KA, Reiser MF, Schoenberg SO (2007) MR imaging in patients with suspected liver metastases: Value of liver-specific contrast agent Gd-EOB-DTPA. Magn Reson Med Sci 6: 43–52
8. Danet IM, Semelka RC, Leonardou P et al (2003) Spectrum of MRI appearances of untreated metastases of the liver. AJR Am J Roentgenol 181:809–817
9. Lee KH, Lee JM, Park JH et al (2013) MR imaging in patients with suspected liver metastases: Value of liver-specific contrast agent gadoxetic acid. Korean J Radiol 14:894–904
10. Choi SH, Lee CH, Kim BH et al (2013) "Nondefect" of arterial enhancing rim on hepatobiliary phase in 3.0-T gadolinium-ethoxybenzyl-diethylenetriamine pentaacetic acid-enhanced liver magnetic resonance imaging: Distinguishing hepatic abscess from metastasis. J Comput Assist Tomogr 37:849–855
11. Demir OI, Obuz F, Sagol O, Dicle O (2007) Contribution of diffusion-weighted MRI to the differential diagnosis of hepatic masses. Diagn Interv Radiol 13:81–86
12. Eun HW, Kim JH, Hong SS, Kim YJ (2012) Malignant versus benign hepatic masses in patients with recurrent pyogenic cholangitis: MR differential diagnosis. Abdom Imaging 37:767–774

13. Muhi A, Ichikawa T, Motosugi U et al (2011) Diagnosis of colorectal hepatic metastases: Comparison of contrast-enhanced CT, contrast-enhanced US, superparamagnetic iron oxide-enhanced MRI, and gadoxetic acid-enhanced MRI. J Magn Reson Imaging 34:326–335
14. Hamm B, Staks T, Muhler A et al (1995) Phase I clinical evaluation of Gd-EOB-DTPA as a hepatobiliary MR contrast agent: Safety, pharmacokinetics, and MR imaging. Radiology 195:785–792
15. Bartolozzi C, Crocetti L, Lencioni R, Cioni D, Della Pina C, Campani D (2007) Biliary and reticuloendothelial impairment in hepatocarcinogenesis: The diagnostic role of tissue-specific MR contrast media. Eur Radiol 17:2519–2530
16. Neri E, Bali MA, Ba-Ssalamah A et al (2016) ESGAR consensus statement on liver MR imaging and clinical use of liver-specific contrast agents. Eur Radiol 26:921–931
17. Merkle EM, Zech CJ, Bartolozzi C et al (2016) Consensus report from the 7th International Forum for Liver Magnetic Resonance Imaging. Eur Radiol 26:674–682
18. Tateyama A, Fukukura Y, Takumi K et al (2012) Gd-EOB-DTPA-enhanced magnetic resonance imaging features of hepatic hemangioma compared with enhanced computed tomography. World J Gastroenterol 18:6269–6276
19. Doo KW, Lee CH, Choi JW, Lee J, Kim KA, Park CM (2009) "Pseudo washout" sign in high-flow hepatic hemangioma on gadoxetic acid contrast-enhanced MRI mimicking hypervascular tumor. AJR Am J Roentgenol 193:W490–W496
20. Granata V, Catalano O, Fusco R et al (2015) The target sign in colorectal liver metastases: An atypical Gd-EOB-DTPA "uptake" on the hepatobiliary phase of MR imaging. Abdom Imaging 40: 2364–2371
21. Lee MH, Kim SH, Kim H, Lee MW, Lee WJ (2011) Differentiating focal eosinophilic infiltration from metastasis in the liver with gadoxetic acid-enhanced magnetic resonance imaging. Korean J Radiol 12:439–449
22. Park MS, Kim MJ, Lim JS et al (2009) Metastasis versus focal eosinophilic infiltration of the liver in patients with extrahepatic abdominal cancer: An evaluation with gadobenate dimeglumine-enhanced magnetic resonance imaging. J Comput Assist Tomogr 33:119–124
23. Chan JH, Tsui EY, Luk SH et al (2001) Diffusion-weighted MR imaging of the liver: Distinguishing hepatic abscess from cystic or necrotic tumor. Abdom Imaging 26:161–165